Diffusion via space discretization method to study the concentration dependence of self-diffusivity under confinement

Marco Sant, George K. Papadopoulos, and Doros N. Theodorou

Additional information on J. Chem. Phys.

Diffusion via space discretization method to study the concentration dependence of self-diffusivity under confinement

Marco Sant, George K. Papadopoulos, and Doros N. Theodorou[a)]
School of Chemical Engineering, National Technical University of Athens, 9 Heroon Polytechniou Street, Zografou Campus, Athens 15780, Greece

The concentration dependence of self-diffusivity is investigated by means of a novel method, extending our previously developed second-order Markov process model to periodic media. Introducing the concept of minimum-crossing surface, we obtain a unique decomposition of the self-diffusion coefficient into two parameters with specific physical meanings. Two case studies showing a maximum in self-diffusivity as a function of concentration are investigated, along with two cases where such a maximum cannot be present. Subsequently, the method is applied to the large cavity pore network of the ITQ-1 (Mobil tWenty tWo, MWW) zeolite for methane (displaying a maximum in self-diffusivity) and carbon dioxide (no maximum), explaining the diffusivity trend on the basis of the evolution of the model parameters as a function of concentration. © *2010 American Institute of Physics*. [doi:10.1063/1.3370344]

I. INTRODUCTION

The aim of this work is to study, through computer simulations, the concentration dependence of self-diffusivity under confinement and, in particular, the physical conditions that can generate a maximum in self-diffusivity as load is increased. For this purpose, we develop a new method, called *diffusion through space discretization* (DSD), applying our second-order Markov process model[1] to periodic media, where the relevant model parameters are obtained during traditional equilibrium molecular dynamics (MD) simulations.[2]

We study the self-diffusivity along only one of the main coordinate directions, the *x*-direction; according to the Einstein relation,[3]

$$D_S = \lim_{t \to \infty} \frac{1}{2} \frac{d}{dt} \left\langle \frac{1}{N} \sum_{i=1}^{N} [x_i(t_0) - x_i(t)]^2 \right\rangle, \tag{1}$$

where x_i is the *x*-coordinate of the *i*th particle as a function of the simulation time t and the brackets stand for averaging over multiple time origins t_0 in the course of an equilibrium simulation.

After introducing the basic theoretical concepts of our DSD method (Sec. II), we present the numerical results for two case studies (see Fig. 1) that can potentially show a maximum in the dependence of the self-diffusivity on loading (Sec. III), followed by two cases that can, by no means, show a maximum. Finally, the DSD method is applied to a real nanoporous material (Sec. IV), studying the self-diffusivity of methane and carbon dioxide inside the large cavity (LC) pore network of ITQ-1 zeolite, the purely sili-

ceous form of MCM-22 (see Fig. 2). A parallel between our method and the widespread transition state theory (TST) approach is presented in Appendix B.

II. THEORETICAL CONCEPTS

A. The second-order Markov process model inside a periodic medium

Starting from our previous work in the bulk,[1] we move now to a periodic medium, redefining the way in which we spatially discretize the system. We call *dividing surface* any surface that divides the system in equal regions of space along the considered coordinate direction (here, *x*) so that a particle is obliged to cross this surface in order to change region (and undergo an effective displacement along *x*). The regions of space between dividing surfaces should have limited extent along the considered coordinate direction; in this way, knowing the region in which a given particle is located corresponds to knowing the *x* coordinate of the particle, with a finite uncertainty.

In any periodic system at equilibrium, with arbitrarily chosen variables specifying its thermodynamic state (here we work in the *NVE*, or microcanonical, and *NVT*, or canonical, ensembles), there is a dividing surface through which the absolute crossing rate (number of particles crossing the surface, in both directions, per unit time) is *minimal* with respect to the other dividing surfaces inside the medium (see Sec. III A for a numerical example). We define this surface as the minimum-crossing surface (MCS). For a given set of system parameters, the location of the MCS is not necessarily unique (e.g. the bulk case); moreover, the location and shape of the MCS can evolve as a function of the state variables. Note that the MCS is not necessarily the surface through which the flux (in each direction) is minimal, or the surface with minimal area: the minimum-crossing, in fact, depends on the product of flux and area.

a)Author to whom correspondence should be addressed. Tel. +30 210 772 3157. FAX: +30 210 772 3112. Electronic mail: doros@central.ntua.gr.
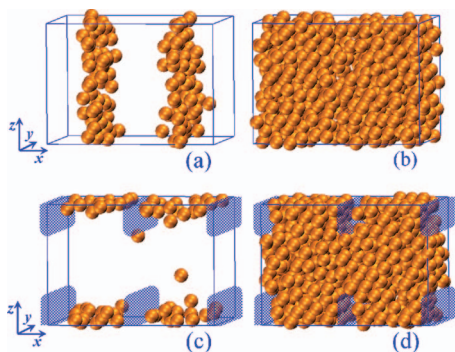
132, 134108-1

FIG. 1. Typical configurations of the sorbate molecules. Case (1) (top): potential wells along the x-direction at low (a) and high (b) density. Case (2) (bottom): potential wells along the z-direction behind uncrossable walls normal to the x-direction, at low (c) and high (d) density.

B. Physical meaning of the model parameters

Using the MCS, we apply our second-order Markov process model (DSD method) to a periodic medium, obtaining a *unique* decomposition of the system self-diffusion coefficient,

$$D_S = \frac{1}{2}\frac{l}{\tau}\zeta, \tag{2}$$

with

$$\zeta = \lim_{i \to \infty}\left(il\frac{P}{1-P}\right)$$

or, from a practical point of view,

$$\frac{1}{\zeta} = \lim_{i \to \infty}\frac{d(1/P)}{d(il)}. \tag{3}$$

In this formalism, l is the distance, along the considered coordinate direction, between two consecutive MCSs, τ is the mean residence time that a particle will spend in each region delimited by two MCSs, and P is the probability that a particle exits each given region of space through the MCS opposite to the one through which it entered. In contrast to the bulk fluid case, the distance l cannot be arbitrarily fixed
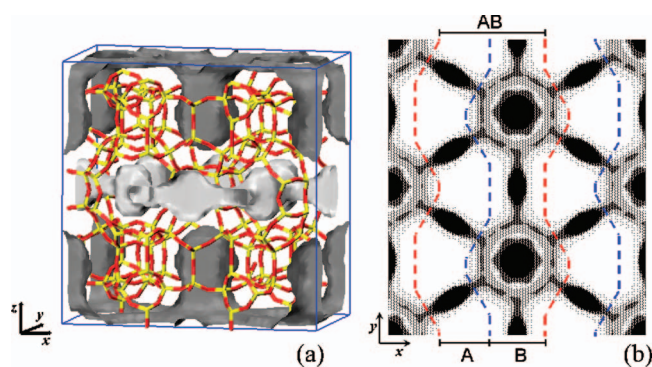

FIG. 2. (a) Accessible volume for CH_4 in ITQ-1 at a total loading of 11.4 molecules/unit cell; the LC system (dark gray) and sinusoidal channel system (light gray) form two independent pore networks. (b) xy projection of CH_4 isodensity surfaces (dark areas denote higher density) in the LC system of ITQ-1 (two unit cells displayed along y). The system is discretized along the x-direction into a sequence of composite AB regions, formed by a region of type A plus one of type B, through MCSs.

but depends on the structure of the medium and its periodicity. For this reason, the limit over bigger regions of space to evaluate the ζ parameter becomes discrete, meaning that it has to be performed by coarse-graining together an increasing number i of primitive regions ($i \in \mathbb{N}$), each one of fixed x-extent l; by definition, a *primitive region* is a region of space bounded by two consecutive MCSs.

The use of the MCS gives a specific physical meaning to the parameters appearing in the expression of the self-diffusion coefficient. In particular, monitoring the dynamics at the location where the crossing between regions is at a minimum (smallest l/τ) ensures that we are observing the motion of only those particles that can most probably achieve a displacement along the considered coordinate direction (greatest ζ). In fact, the transmission probability P defined with respect to the MCS is higher than the transmission probability defined with respect to any other location of the dividing surface inside the system. This fact comes from Eq. (2) since l/τ and ζ will rearrange according to the location of the dividing surface in order to give the correct self-diffusivity value (see Sec. III A for a numerical example).

1. The α parameter

In our previous work we have seen that

$$l/\tau = \langle|v_x|\rangle\alpha, \tag{4}$$

where $\langle|v_x|\rangle$ is the mean translational speed of the particles along the x-direction (at equilibrium, in general, the particles' velocities follow a Maxwell–Boltzmann distribution and we have $\langle|v_x|\rangle = \sqrt{2k_BT/\pi m}$). The $\alpha(T,\rho)$ parameter is a dimensionless quantity accounting for the efficiency of the thermal speed (with respect to the bulk fluid where $l/\tau = \langle|v_x|\rangle$) in bringing about transitions across the MCSs. By the definition of the MCS, one always has $\alpha \leq 1$, with the equality holding in the bulk case.

Following our work in the bulk, see also Appendix A, we can write

$$\alpha = \frac{L}{N}\int_{\text{MCS}} c(x,y,z)dS, \tag{5}$$

where the integral is now performed over the MCS (which can have any orientation and shape). Here, L is the length of the simulation box along the considered direction (by construction an integer multiple of l), $c(x,y,z)$ is the particle number density as a function of position in space, and N is the number of particles inside the box, satisfying the normalization condition $N = \int_V c(x,y,z)dxdydz$, where V is the accessible volume. We will use the symbol $\rho = N/V$ to denote the mean number density in the system; for a given porous medium and a given single-component sorbate fluid, once ρ and T are specified, the entire density distribution $c(x,y,z)$ is set at equilibrium.

Since $S = \int_{\text{MCS}} dS$ is the surface of the MCS, α can be thought as the ratio of $(1/S)\int_{\text{MCS}} c(x,y,z)dS$ (the mean density at the MCS) and $\rho^* = N/(LS)$ (the mean density at the MCS in an ideal bulk system of volume $V^* = LS$, homogeneously filled with N particles). From this point of view, α measures the *fraction* of sorbate that can *see* the crossing-

limiting window for diffusion along the given direction (global bottleneck for the rate of region change) with respect to the ideal bulk conditions (where the entire load N would see the window). This fraction depends on the profile of the sorbate probability density (thermodynamic factor), which can generate an energetic barrier, and on the geometry of the region (geometric factor), which can generate an entropic barrier.

2. The ζ parameter

The parameter $\zeta(T,\rho)$ is a characteristic length accounting for the particle-particle collisions and the tortuosity of the system, which can prevent a particle from successfully traversing the whole region. In particular, this parameter is a *monotonically decreasing function* of ρ. Note that also the particle-particle collisions depend on the profile of the sorbate density distribution (in denser regions there are more collisions).

From here on, we will consider the temperature T of the system to be fixed, thus focusing our attention on the evolution of $\alpha(\rho)$ and $\zeta(\rho)$ as functions of density.

C. Effects of a periodic medium

Applying our second-order Markov process model, we should consider the differences between a periodic medium and the bulk. For simplicity, in this work we treat only the case of a rigid (not thermally fluctuating) periodic medium. The presence of the medium modifies the sorbate density distribution, which becomes inhomogeneous due to the sorbate-sorbent interactions. We separate these interactions in two groups: (a) *potential wells* and (b) *uncrossable walls*; according to the kind of inhomogeneities they generate in the density distribution of the sorbate. The potential wells, due to their finite depth, generate inhomogeneities in the equilibrium density distribution, which are concentration dependent, and will disappear at infinite loading. The uncrossable walls, on the other hand, generate inhomogeneities in the density distribution, which, practically, do not depend on loading.

The potential wells have a different effect on diffusivity, depending on their orientation and position with respect to the MCSs. In the following case studies, the MCSs will be, by construction, normal to the diffusion coordinate. At the same time, the potential wells will be oriented either along or perpendicular to the diffusion coordinate; the periodic arrangement of uncrossable walls, on the other hand, will always be along the diffusion coordinate, the walls themselves acting perpendicularly to that direction (see Fig. 1).

D. Load redistribution process

To understand the concentration dependence of self-diffusivity in a periodic medium, we should investigate the evolution of the sorbate density distribution inside the sorbent, as load is increased. When there are no potential wells, the sorbate tends to fill homogeneously the accessible volume. On the contrary, if potential wells are present, the density distribution will be spatially inhomogeneous, with re-

gions where the concentration of the sorbate is higher (inside the wells) and regions where the concentration is lower (outside the wells). In this case, a *load redistribution* process will take place inside the sorbent as load is increased. By load redistribution, we mean an evolution of the density profile toward homogeneity over the whole accessible volume due to filling of the potential wells by sorbed particles. Using the definition of sorbate probability density function (PDF), $f(x,y,z) = c(x,y,z)/N$, the previous considerations apply also to the evolution of the free energy profile, $A(x,y,z)$, through the relation

$$A(x,y,z) = -k_{\rm B}T\,\ln[f(x,y,z)], \tag{6}$$

in agreement with the work of other authors.[4]

The load redistribution will always take place, independently of the kind of sorbate; still, the sorbate-sorbate interactions can affect the rate of change in the density profile with respect to load increase.

E. Favorable conditions for a maximum in $D_{\rm S}$

As we have stated, at constant temperature, $\zeta(\rho)$ is a monotonically decreasing function of load. In fact, the transmission probability P to cross the whole region and exit through the MCS opposite to the one through which the particle has entered can only decrease if the number of particles inside the region (between two subsequent MCSs) grows, due to the higher chance to have a collision that inverts the direction of motion of the traversing particle.

Since $\zeta(\rho)$ is a monotonically decreasing function, the necessary but not sufficient condition to have a maximum in $D_{\rm S}$, as a function of load, is to have an increase in $\alpha(\rho)$; then, a maximum appears *if and only if* the growth with load of the α parameter is faster than the corresponding decrease in the ζ parameter.

In the next case studies, we isolate two scenarios that could lead to an increase in $\alpha(\rho)$, both of them based on the load redistribution process.

(1) *Potential wells arranged along the diffusion coordinate.* This situation is shown pictorially in Fig. 1(a). The well will generate a gradient in the sorbate PDF along the considered coordinate direction, i.e., $\nabla_x f(x,y,z) \neq 0$. Then, as the load is increased, the particles will fill the well and start occupying the regions outside the well, forcing the local density at the MCS to increase, $\lim_{\rho\to\infty} \nabla_x f(x,y,z) \approx 0$ [see Fig. 1(b)].

To study the evolution of the α parameter as a function of loading, we can either look at the sorbate density distribution, $c(x,y,z)$, or the sorbate PDF, $f(x,y,z)$, since we are interested in the gradient of these quantities along the diffusion direction and, in particular, in how this gradient changes with increasing loading. Then, to compare together different loading conditions at a glance, it is more convenient to use the sorbate PDF, which is normalized (see the work on ITQ-1 in Sec. IV). If interested in the load dependence of the ζ parameter, on the other hand, one has to look at the sorbate density distribution, $c(x,y,z)$, since we are interested in its actual value and not its gradient.
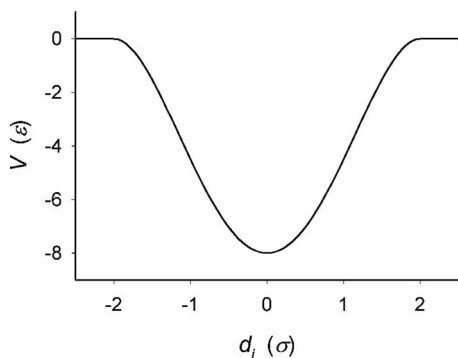
FIG. 3. Profile of the potential well.

(2) *Potential wells arranged perpendicularly to the diffusion coordinate and located behind uncrossable walls.* This situation is shown pictorially in Fig. 1(c). The presence of an uncrossable wall generates a (loading independent) inhomogeneity in the sorbate PDF along the x-direction. The potential well, on the other hand, generates a (loading dependent) inhomogeneity perpendicular to the x-direction (here, along z) so that $\nabla_z f(x, y, z) \neq 0$. The uncrossable wall reduces the size of the window connecting adjacent regions, while the potential well removes part of the load from the window, hiding it behind the uncrossable wall. All this decreases the fraction of load that can see the MCS. At higher loadings then, when the well gets filled, more sorbate will tend to occupy the region of space in front of the MCS, increasing the value of α [Fig. 1(d)].

III. RESULTS

A. Potential wells arranged along the diffusion coordinate

To analyze the effect of potential wells along the diffusion coordinate, x, we use the computational tools developed during our previous work in the bulk.[1] In particular, we perform equilibrium MD simulations in the microcanonical (NVE) ensemble using, for the particle-particle interaction, the repulsive part of the Lennard-Jones potential, truncated and shifted at the minimum (Weeks–Chandler–Andersen, WCA, potential)[5]

$$U(r_{ij}) = \begin{cases} 4\varepsilon\left(\dfrac{\sigma^{12}}{r_{ij}^{12}} - \dfrac{\sigma^{6}}{r_{ij}^{6}}\right) + \varepsilon, & r_{ij} \leq 2^{1/6}\sigma \\ 0, & r_{ij} > 2^{1/6}\sigma. \end{cases} \quad (7)$$

In addition, we introduce an attractive position-dependent potential energy field (i.e., a potential well),

$$V(d_{i}) = \begin{cases} \dfrac{\varepsilon}{2}\left(8\dfrac{d_{i}^{2}}{\sigma^{2}} - \dfrac{d_{i}^{4}}{\sigma^{4}} - 16\right), & d_{i} \leq 2\sigma \\ 0, & d_{i} > 2\sigma, \end{cases} \quad (8)$$

where $d_{i} = x_{i} - x_{\text{well}}$ is the x-distance of the ith particle from the center of well located at x_{well}. The parameters of the well are chosen to ensure continuity of forces between regions with and without potential (see Fig. 3). The well has a width

of 4σ and a depth of 8ε. To sample different well depths, we multiply the $V(d_{i})$ potential by a constant g, which is assigned the values 0, 0.5, and 1.

The system is constituted from unit cells with dimensions of $14\sigma \times 10\sigma \times 10\sigma$, each unit cell hosting two potential wells. The centers of the wells are located at distances $x_{\text{well 1}} = 3.5\sigma$ and $x_{\text{well 2}} = 10.5\sigma$ from the left border of the unit cell, arranged symmetrically with respect to the center of the unit cell [see Fig. 1(a)]. This creates a periodic potential along x, with period 7σ. Periodic boundary conditions (PBCs) are applied along the three coordinate directions. In the following computations, all property values are reported in corresponding Lennard-Jones reduced units. The runs are performed with a simulation time step $\delta t = 0.002(m\sigma^{2}/\varepsilon)^{1/2}$, for a total number of 5×10^{7} steps. The temperature is the same for all the runs; all systems are carefully pre-equilibrated at $T = 1.00\varepsilon/k_{B}$.

1. Transmission probability computation

As a general procedure, to compute the transmission probability P_{il} associated with regions of x-extent il, $i \in \mathbb{N}$, we divide the simulation box along the considered direction into an integer number L/il of identical regions (separated by MCSs), and index the regions. At every step, we check the position of each particle, determining in which region it is located; in this way each particle gets a *discrete position* through the region index. During the next simulation steps, if the discrete position of a particle changes, this means that a MCS has been crossed. The crossing can occur while traveling: either along the positive (change in the discrete position index equal to +1), or negative (change in the discrete position index equal to −1), x-direction. This information is stored and used at the next crossing (of the same particle) to determine which *kind of event* has taken place: we accumulate the number of *transmission events* (a particle crossing a MCS in the same direction as its previous crossing), as opposed to the *reflection events* (a particle crossing in the opposite direction with respect to its previous crossing). The ratio between the number of transmission events and the total number of events, for regions of extent il, gives the corresponding transmission probability P_{il}.

At the beginning of the simulation, to ensure that a steady value for the ratio between transmissions and reflections has been attained, we should wait until every particle has managed at least one crossing, so that each region is filled with particles of which we know the direction of their previous crossing; otherwise, an abundance of reflection events with respect to transmission events is found. On the other hand, in systems where the confinement of sorbate molecules is very strong (some particles spending most of the simulation time in just one region), this requirement would be too strong: the time needed for *all* the particles to make at least one crossing, in fact, is size dependent (it increases with the size of the simulation box). To avoid this problem, in these cases we wait for only a considerable fraction, e.g., 99%, of the total loading to make at least one crossing.
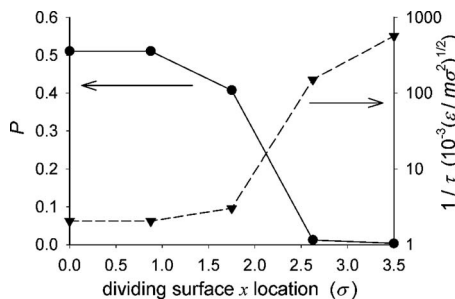
FIG. 4. Dependence of the transmission probability P (circles), and of the inverse of the mean residence time, $1/\tau$ (triangles), on the location of the dividing surface along the x coordinate (measured starting from the left border of the unit cell). The system is loaded with 125 WCA spheres with a well depth parameter $g=1$. The first well is centered at $x_{well\ 1}=3.5\sigma$. The x-extent of the primitive region is $l=7\sigma$.

2. Mean residence time computation

We discretize the simulation box, of x-length L, into an integer number $n_r=L/il$ of regions with x-extent il, where i is an arbitrarily chosen integer and l is the x-extent of the primitive region. During the simulation, then, we compute the mean residence time, $\tau_{il}=\Delta tN/\text{exits}$, that a particle spends, on average, in a given region of x-extent il: this is simply the total simulation time, Δt, multiplied by the total number of particles inside the simulation box, N, and divided by the number of particles' exits (from both boundaries of all the n_r regions) accumulated during the simulation, exits $=\Sigma_{k=1}^{n_r}\text{exits}_k$, where k is simply an index of the various regions. As we can see, the mean residence time τ_{il} increases linearly with the x-extent il of the region (since n_r, and so exits, are inversely proportional to il). From here on, we will simply speak of the mean residence time τ, associated with the primitive region (of x-extent l), omitting the subscript. By definition, the number of exits from a region (of any extent), through both its boundaries, is equivalent to the absolute number of crossings through a single MCS, in both directions. Note the *local* nature of the mean residence time, which depends only on the crossings at the MCSs, as opposed to the transmission probability, which is evaluated over the *whole* region (or more regions coarse grained together).

3. MCS location

In this specific material, any plane perpendicular to the x-direction and located outside the potential wells is an MCS. To visualize this fact, we perform some preliminary runs discretizing the system in regions of x-extent $l=7\sigma$ (in view of the periodicity of the system), using two dividing surfaces, perpendicular to the x-direction, in each unit cell. We study how the transmission probability, P, and the inverse of the mean residence time, $1/\tau$, change with the location of the dividing surfaces. This location is parametrized as the x distance, from the left border of the unit cell, at which the first dividing surface is placed, the second dividing surface being always located at a x-distance 7σ from the first one. In Fig. 4 we see the corresponding plots at a fixed load of 125 WCA spheres per unit cell, with a well depth parameter $g=1$. The minimal crossing of the dividing surfaces

(lowest $1/\tau$) is found for the planes located outside the wells; these are the MCSs. At the same time, with the MCS space discretization we obtain the highest transmission probability value, P (see Fig. 4). Our DSD method gives an acceptable value of self-diffusivity with any of the above discretizations, but the parameters computed using the MCSs are the ones that minimize the errors related to the correlation over consecutive transmission events.

4. Main computations

For the following simulations, we chose two MCS for each unit cell: one located at the left border ($x=0\sigma$) and one at the center ($x=7\sigma$) of the unit cell. We vary the load of each unit cell from 125 to 1250 spherical WCA particles to sample different densities; for all the runs, we keep the number of particles in the simulation box between 750 and 1250, choosing the number of unit cells accordingly.

Beside the mean residence time and the transmission probability, during each run we also compute the particles' mean absolute velocity along the x-direction $\langle|v_x|\rangle$; in all our runs we have $\langle|v_x|\rangle=\sqrt{2.00\varepsilon/\pi m}$. This value is used during the data postprocessing to obtain the α parameter through Eq. (4). Statistical errors are computed through the standard deviation over three consecutive runs for each system. In all our plots the lines are to guide the eye; the error bars, where not visible, are smaller than the symbol size.

In Fig. 5(a) we can see the evolution of the α parameter as loading increases, for the three different well depths g. In the case $g=0$, no potential well is present and the system is simply a bulk fluid; then, as expected, the particles cross the MCS taking full advantage of their thermal speed so that $l/\tau=\langle|v_x|\rangle$ and $\alpha=1$ for all loadings. For the system with $g=0.5$, we observe a clear increase in the α parameter as load grows, and this is even more pronounced in the case of $g=1$. As explained in Sec. II D, this increase in α comes from the redistribution of the load inside the unit cell as the number of particles grows [compare (a) and (b) in Fig. 1]: after filling the potential wells, the additional particles populate also the regions outside the wells, making the particles' PDF more homogeneous along the x-direction (smoother free energy profile), and thus enhancing the transfer of matter between adjacent regions. In this specific system, a reliable estimate of ζ can be obtained using just P_l and P_{2l} (see Table I). According to Eq. (3), for $i=1,2$, we get

$$1/\zeta = (1/P_{2l} - 1/P_l)/l. \tag{9}$$

In Fig. 5(b) we see the evolution with loading of the ζ parameter, where the monotonic decrease of the ζ function with increasing loading can be clearly appreciated. This decrease is greater for higher values of the well depth parameter g. To test the accuracy of our formulation,

$$D_S = 0.5\langle|v_x|\rangle\alpha\zeta, \tag{10}$$

self-diffusivity values computed from α and ζ via Eq. (10), shown with open symbols in Fig. 5(c), are compared against self-diffusion coefficients computed through the traditional mean squared displacement (MSD) routine, shown with cross symbols in Fig. 5(c); note the excellent agreement ob-
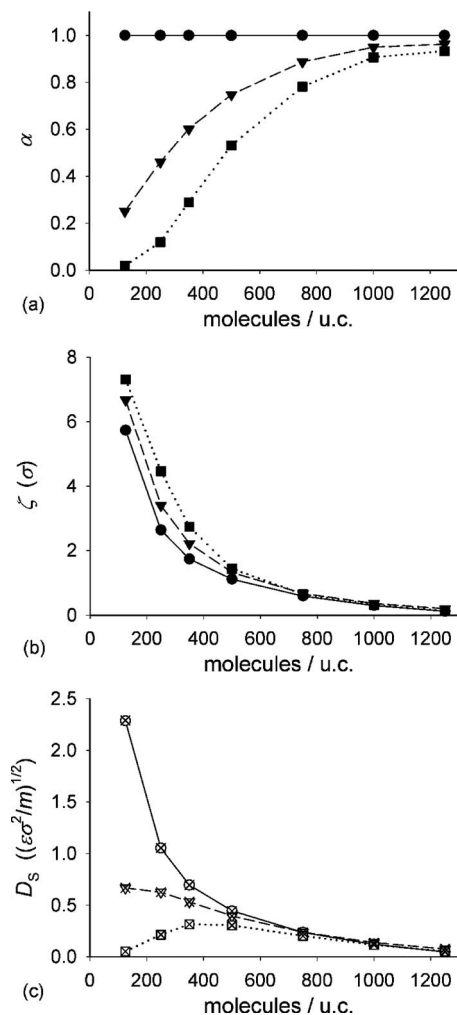
FIG. 5. Evolution of the α parameter with loading (a), for three different well depths: $g=0$ (circles), $g=0.5$ (triangles), and $g=1$ (squares). Same plot for the ζ parameter (b). Loading dependence of the self-diffusivity (c), computed through DSD equation (10), with $\langle |v_x| \rangle = \sqrt{2.00\varepsilon/\pi m}$, for the three well depths (open symbols), and corresponding MSD results (crosses).

tained in all cases. For the $g=1$ well depth, we see that the self-diffusion coefficient goes through a maximum as loading increases, open squares and crosses in Fig. 5(c). As mentioned in see Sec. II E, for constant $\langle |v_x| \rangle$, the increase in α with loading is a necessary but not sufficient condition to have a maximum in the self-diffusion coefficient with respect to loading: we need the increase in α to be faster than the

corresponding decrease in ζ; this is the case for our model system with $g=1$, but not with $g=0.5$.

To analyze the accuracy of our method, in Table I we compare computed self-diffusivities along the x-direction coming from the standard MSD procedure, our formulation using only one region $D_S = 0.5 \langle |v_x| \rangle \alpha l P_l / (1-P_l)$, (DSD1), and two regions $D_S = 0.5 \langle |v_x| \rangle \alpha l / (1/P_{2l} - 1/P_l)$, (DSD2). We also show the corresponding percentile statistical errors coming from the standard deviation over three consecutive runs (E%). In the last two columns, we give the percentile absolute difference between the MSD and our formulation using only one region, $\Delta 1\%$, and between the MSD and our formulation using two regions, $\Delta 2\%$. The system used for these computations is a bulk, $g=0$, with primitive region of x-extent $l=7\sigma$; the loading ranges from 125 to 1250 WCA spheres per unit cell. Note how $\Delta 1\%$ decreases at high densities, where the high number of collisions enables a reliable computation of D_S using the transmission probability over only the primitive region (weak correlation on consecutive transmissions); for systems with enhanced collisionality this is true also at lower loadings. Even though the statistical errors are small, the choice of the simulation box size (number of unit cells along x, y, and z) may lead to different results in the self-diffusion coefficient (size effects), within 3%.

B. Potential wells arranged normally to the diffusion coordinate, located behind uncrossable walls

This system is characterized by three kinds of interactions: the *particle-particle* interaction, the *potential well-particle* interaction, and the *uncrossable wall-particle* interaction. For the particle-particle interaction, we use the WCA potential as in the previous case study. As potential well we use the same shape of Fig. 3, but this time we change the orientation of the periodic series of wells, arranging them along the z-direction. The interaction coordinate becomes $d_i = z_i - z_{\text{well}}$, i.e., the z-distance between the ith particle and the center of the well z_{well}. The system is composed of unit cells with dimensions of $14\sigma \times 10\sigma \times 10\sigma$. We fix the centers of the wells to be located at the upper and lower z-border of each unit cell, e.g., $z_{\text{well}} = \pm 5\sigma$ when the unit cell is centered about the origin.

For the uncrossable wall, we use a WCA (Ref. 5) shaped potential,

TABLE I. Self-diffusivity computations along the x-direction for various loadings: MSD procedure, our formula using only one region (DSD1), and two regions (DSD2) (see text); with their corresponding percentile statistical errors, E%. The last two columns give the percentile absolute difference between: MSD and DSD1, $\Delta 1\%$; MSD and DSD2, $\Delta 2\%$.

$N/$uc	MSD	E%	DSDl	E%	DSD2	E%	$\Delta 1\%$	$\Delta 2\%$
125	2.289	0.13	2.100	0.02	2.285	0.09	8.3	0.18
250	1.054	0.12	1.003	0.06	1.052	0.04	4.8	0.17
350	0.6953	0.4	0.6742	0.12	0.6940	0.3	3.0	0.19
500	0.4435	0.2	0.4302	0.08	0.4442	0.2	3.0	0.17
750	0.2365	0.4	0.2300	0.14	0.2367	0.5	2.7	0.09
1000	0.1195	0.2	0.1179	0.02	0.1194	0.2	1.3	0.11
1250	0.047 84	0.2	0.047 97	0.2	0.047 99	0.08	0.3	0.3

$$U(w_i) = \begin{cases} 4\varepsilon \left(\dfrac{\sigma^{12}}{w_i^{12}} - \dfrac{\sigma^6}{w_i^6} \right) + \varepsilon, & w_i \leq 2^{1/6}\sigma \\ 0, & w_i > 2^{1/6}\sigma \end{cases} \quad (11)$$

with

$$\begin{cases} w_i = x_i - x_{\text{wall}} & \text{if } z_i^2 > 9\sigma^2 \\ w_i = [(x_i - x_{\text{wall}})^2 + (z_i - 3\sigma)^2]^{1/2} & \text{if } 0 < z_i \leq 3\sigma \\ w_i = [(x_i - x_{\text{wall}})^2 + (z_i + 3\sigma)^2]^{1/2} & \text{if } -3\sigma \leq z_i \leq 0, \end{cases} \quad (12)$$

where x_i and z_i are the coordinates, along the corresponding directions, of the ith particle inside the unit cell, which is assumed here to be centered at the origin. In this formalism, x_{wall} takes the values -7σ, 0, and 7σ (left x-border, center, and right x-border of the unit cell). Thus, a series of slits perpendicular to the x-direction is generated, with period 7σ. The slits have an interaction-free window of size $(6-2^{1/6})\sigma$ [see Figs. 1(c) and 1(d)]. From a heuristic point of view, the uncrossable wall potential can be thought of as emanating from imaginary spheres, which interact with the sorbate molecules through a WCA potential. At the top and bottom sections of the unit cell, each of thickness 2σ along the z-direction, upon approaching a wall, a sorbate molecule *sees* an imaginary sphere within the wall, with its center at the same y and z coordinates as the molecule itself. In the middle section of the simulation box, of thickness 6σ, the sorbate molecule sees only the imaginary sphere at the edge of the wall (where the window begins), whose center lies at the same y coordinate as the molecule itself, while its z coordinate is either 3σ or -3σ; each particle sees only one imaginary sphere at a time, the one located at the closest distance, within the wall locus, from the particle itself. The mass of the imaginary spheres is considered to be infinite so that only the sorbate molecule's motion is affected by the wall force. This technique allows us to generate pseudomaterials of any shape, conserving the total energy of the sorbate phase.

We vary the load of each unit cell from 75 to 1000 spherical WCA particles, with a total number of particles in the simulation box between 600 and 1000. For the rest, the simulation is performed exactly as in the previously investigated case (Sec. III A), using three different well depths g (0, 0.5, and 1), with the system pre-equilibrated at $T = 1.00\varepsilon/k_B$.

In Fig. 6, we can see the increase in the α parameter for all the three well depths; the one for $g=1$ is most pronounced [plot (a)]. Even in the case with $g=0$ (no potential wells along z), a small growth of α with loading is observed, most probably due to the increase in accessible volume (effective widening of the slit window) at higher loadings; in any case, the α parameter is far away from bulk conditions ($\alpha=1$), due to the uncrossable walls which reduce the area of the MCSs. The ζ parameter, shown in Fig. 6(b), is a monotonically decreasing function of loading. Apart from the first two points (see next paragraph), ζ has been computed using the formula over only two primitive regions, Eq. (9). Finally, in plot (c) we display the self-diffusivity computed through our DSD formulation [Eq. (10)] with $\langle |v_x| \rangle = \sqrt{2.00\varepsilon/\pi m}$ and through
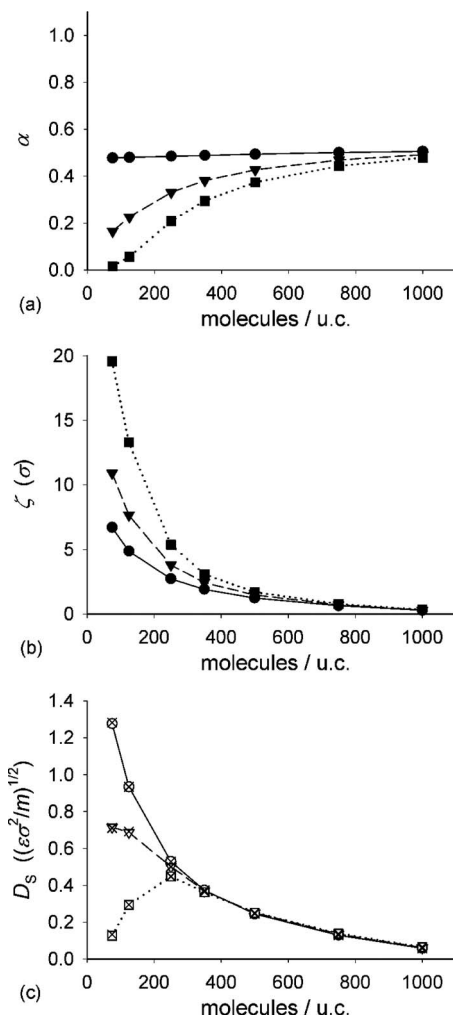

FIG. 6. Same as Fig. 5 for the system with potential wells arranged normally to the diffusion coordinate and located behind uncrossable walls.

the usual MSD procedure. A maximum in the dependence of self-diffusivity over loading is found for the well depth $g=1$.

At low loadings (i.e., 75 and 125 molecules/unit cell), we noticed a strong correlation in the moves of the particles performing consecutive transmission events, due to the low sorbate density in the zone facing the MCSs, with consequent low probability for a molecule to suffer a collision that can invert (randomize) its velocity along the x-direction. For these two loadings, the ζ parameter has been computed according to Eq. (3), with a number of primitive regions coarse grained together, i, ranging from 2 to 10. Note that, due to computational limitations, the simulation box cannot contain too many primitive regions along the x-direction. To apply Eq. (3) for values of i that exceed the simulation box, then, during the runs, we store a *discrete trajectory* for each particle; this is made of two integers for each event regarding the given particle: the *kind of event* performed and the *time step* at which this occurred. For the kind of event we use $(+1)$ for a transmission along the positive x-direction, (-1) for a transmission in the negative direction, $(+5)$ for the reflection of a particle that was previously traveling along the positive x-direction, and (-5) for the reflection of a particle that was previously traveling in the negative x-direction.
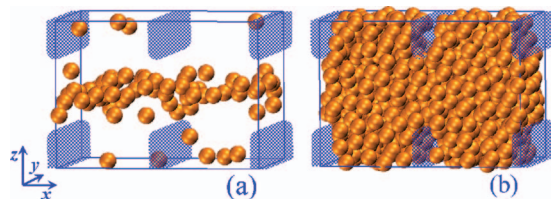
FIG. 7. Potential wells along the z-direction, traversing the MCS, plus un-crossable walls normal to the x-direction, at low (a) and high (b) density.

With this information, during post processing, we can reproduce all the particles dynamics, in a coarse grained fashion; in particular, we can consider the particles as traversing regions of x-extent greater than the simulation box, thus removing the correlation over consecutive transmission events. This procedure is solely intended to increase the accuracy of our DSD method, allowing the achievement of the same results as the MSD procedure (taken as reference); it cannot remove the systematic errors related to system size effects, occurring when the simulation box is too small.

C. Cases that cannot generate a maximum in self-diffusivity as a function of loading

We present now two case studies where the α parameter does not grow with loading; consequently there is no chance to observe a maximum in the self-diffusivity curve. The two new cases are (3) potential wells along the x-direction, while the diffusivity is studied along the y-direction (primitive region of $l_y = 5\sigma$), same configuration as in Figs. 1(a) and 1(b); and (4) potential wells along the z-direction traversing the MCS (i.e., $z_{well} = 0$ in a unit cell centered about the origin), plus uncrossable walls normal to the x-direction (see Fig. 7), while the diffusivity is studied along the x-direction with a primitive region of x-extent $l = 7\sigma$. Both systems have a well depth parameter $g = 0.5$; the remaining simulation details are exactly as the ones used, respectively, for case studies (1) and (2) in the Secs. III A and III B.

In Fig. 8(a) we see the evolution of the α parameter for these two cases: in case (3), the α along the y-direction is unaffected by the presence of the wells along the x-direction, then we obtain the same result as in a bulk fluid ($\alpha = 1$); in case (4) the presence of the wells along z forces most of the molecules to face the MCSs at low densities, then, as load is increased and the wells are filled, additional molecules occupy also the space in between the uncrossable walls (load redistribution), hindering the diffusion along the x-direction. The ζ parameter, as expected, decreases monotonically with loading for both cases [Fig. 8(b)]. Note that for case (3) [compare with circles in Fig. 5(b)], the presence of the well along x affects the ζ parameter along y (unlike what happens for the α parameter, where the well has no influence). At low loadings the ζ parameter has been computed by postprocessing the sorbate *discrete trajectory* according to Eq. (3), while for higher loadings Eq. (9) has been used. In plot (c) we compare the self-diffusivity coming from DSD equation (10), having $\langle |v_{x,y}| \rangle = \sqrt{2.00\varepsilon/\pi m}$, with the standard MSD one.
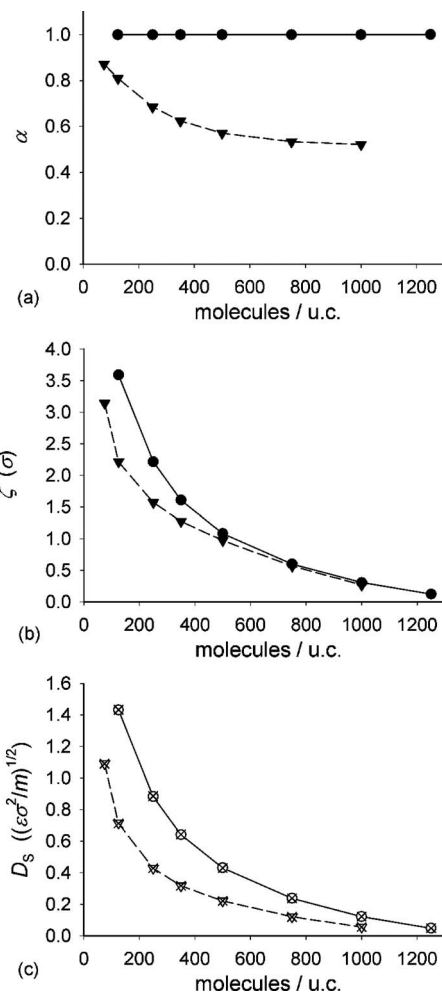

FIG. 8. Two other case studies: (3) potential wells along the x-direction, study of the self-diffusivity along y (circles); and (4) potential wells along the z-direction, traversing the MCS, plus uncrossable walls normal to the x-direction, study of the self-diffusivity along the x-direction (triangles). Evolution with loading of the α parameter (a) and of the ζ parameter (b). Loading dependence of the self-diffusivity (c), computed through DSD equation (10) (open symbols), and corresponding MSD results (crosses).

IV. APPLICATION TO A REAL MATERIAL

The theoretical concepts developed in the previous sections can be applied also to real materials. Here we focus our attention on a nanoporous sorbent, giving a numerical example for the study of the self-diffusivity of CH_4 and CO_2 inside the LC network system of the ITQ-1 zeolite.[6]

Most of the time, the potential wells found in nanoporous materials have a spheroidal shape, with limited extent in space along all the three main coordinates; such wells are addressed as *sorption sites*. Looking at the mechanisms through which these sorption sites prevent molecules from reaching the MCSs, we find that an increase in the α parameter can be achieved in exactly the same ways seen in Sec. II E; in particular (1) if the sites *face* the MCSs for the given coordinate direction, where a site *faces* a MCS if it is in front of it, without traversing it, and (2) if the sites are screened behind uncrossable walls with respect to the MCSs.

In some periodic materials, such as zeolites, the use of MCSs to subdivide the system may result into an alternation, along the considered diffusion direction, of two different

types of primitive regions: A and B. In Fig. 2(b) we can see the discretization through MCSs, along the x-direction, of the LC pore network of the ITQ-1 zeolite filled with methane: region A is formed by two *narrow necks* per unit cell, while region B by a *supercage* and a *narrow neck* per unit cell; in each unit cell there are two regions A and two regions B. To study the diffusivity in such systems using our DSD coarse graining method, we can simply consider the two regions A and B as parts of one large composite region AB. Then, the self-diffusivity along the x-direction comes from

$$D_S = \frac{1}{2} \frac{l_{AB}}{\tau_{AB}} \zeta_{AB}, \qquad (13)$$

where $l_{AB} = l_A + l_B$ is the total length of the AB region and $\tau_{AB} = \tau_A + \tau_B$ is the total mean residence time a particle spends in the AB region. We have $1/\zeta_{AB} = \lim_{i \to \infty}[d(1/P_{AB})/d(il_{AB})]$, where the limit for the transmission probability is taken over an increasing integer number i of AB regions coarse grained together. At equilibrium, we can write $l_{AB}/\tau_{AB} = \langle|v_x|\rangle \alpha_{AB}$, with $\alpha_{AB} = (l_{AB}/N_{AB})\int_{MCS} c(x,y,z)dS$, $N_{AB} = N_A + N_B$ being the total number of molecules inside the AB region.

A. Self-diffusivity of CH_4 and CO_2 in the LC pore network of ITQ-1

In our recent work on methane and carbon dioxide inside ITQ-1 zeolite at 300 K,[7] we have observed a maximum in the dependence of the self-diffusivity on loading for CH_4 inside the LC pore network, while the diffusivity of CO_2 shows simply a monotonic decrease [Fig. 9(c)]. All simulation details are reported elsewhere.[7] In particular, to have convenient PBCs we use a double unit cell instead of the original hexagonal one. The new unit cell has an orthorhombic shape, with axes: $a = 2.4609$ nm, $b = 1.4208$ nm, and $c = 2.4945$ nm. In each unit cell there are two supercages and six narrow necks (see Fig. 2). Applying our DSD method to the composite AB regions, we can see that the α_{AB} parameter goes through a maximum in the case of CH_4, while it exhibits a decrease followed by a slight increase for CO_2 [Fig. 9(a)]; at the same time, the ζ_{AB} parameter decreases monotonically for both sorbates, as expected from Sec. II B.

1. DSD in the LC of ITQ-1

To discretize space we use the following procedure: at each step, invoking ad hoc PBCs, we rescale the coordinates of all the molecules in the simulation box to their corresponding positions inside the primitive unit cell. At this point, we check if the molecules are inside the necks: we draw a circle of appropriate radius, R_{neck}, around each neck and check if the xy coordinates of the molecules lie within this circle [see Fig. 11(a)]. If this is the case, we assign the value 0 to the *discrete position* of the molecule under investigation (a value for each molecule), otherwise we assign the value 1. At each step, then, we compare the actual discrete position of the sorbate molecules with the one they had at the previous step. If this has changed, we know that a crossing has taken place: from a supercage to a neck if the change in discrete position equals -1, and vice versa if the change in
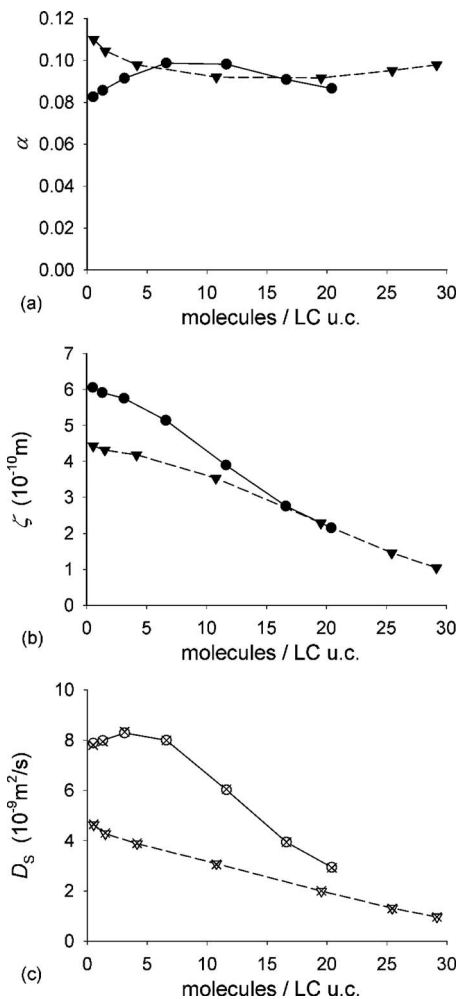

FIG. 9. CH_4 (circles) and CO_2 (triangles) in the ITQ-1 LC pore network for various loadings at 300 K; α_{AB} parameter (a), ζ_{AB} parameter (b), self-diffusivity (c) from DSD equation (13) (open symbols), and corresponding MSD (crosses), where $\langle|v_x|\rangle_{CH_4} = 3.15 \times 10^2$ m/s and $\langle|v_x|\rangle_{CO_2} = 1.90 \times 10^2$ m/s.

discrete position equals $+1$. A supercage has six possible exits. When a molecule crosses, we check in the neighborhood of which exit this happens (we use a circle, centered at the given MCS, to check if the molecule lies within). In this way, to each crossing molecule is assigned a *discrete exit* value, ranging from 1 to 6 according to the exit that has been used. At this point, we have full control on the discrete dynamics of the sorbate molecules within the LC of ITQ-1; in particular, we can compute the mean residence time, τ, and transmission probability, P, as in the previously investigated case studies. Note that, for the diffusion along the x-direction, only 4 out of the 6 exits of each supercage are relevant [see Fig. 2(b)]. A rigorous procedure to locate the exact shape and position of MCSs within the unit cell is currently under development. The MCSs presented here are chosen through careful study of the sorbate PDF and an optimization over various radii for each sorbate; as an approximation, we keep the location of the MCSs fixed for all loadings.

During each simulation, we also compute the mean number of molecules within all the narrow necks, N_{necks}, and

within all the supercages, N_{cages}, of the simulation box. From these values we obtain the mean number of molecules, per unit cell, in each region A and B,

$$\begin{cases} N_A = [2N_{necks}/3]/(2n_{uc}) \\ N_B = [N_{cages} + (N_{necks}/3)]/(2n_{uc}), \end{cases} \quad (14)$$

where n_{uc} is the number of unit cells in the simulation box.

2. Methane diffusivity

We focus our attention on CH_4; to understand what provokes the increase with loading of its α_{AB} parameter, we should consider the contribution of each single region A and B to the overall α_{AB},

$$\begin{aligned} \alpha_{AB} &= \frac{l_A + l_B}{N_{AB}} \int_{MCS} cdS \\ &= \frac{l_A}{N_A} \frac{N_A}{N_{AB}} \int_{MCS} cdS + \frac{l_B}{N_B} \frac{N_B}{N_{AB}} \int_{MCS} cdS \\ &= \left[\alpha_A \frac{N_A}{N_{AB}} \right] + \left[\alpha_B \frac{N_B}{N_{AB}} \right], \end{aligned} \quad (15)$$

studying the evolution of α_A and α_B, together with the evolution of the *load fraction* in the same regions, N_A/N_{AB} and N_B/N_{AB}.

In Fig. 10 we can see that the greatest contribution to the overall increase in α_{AB} comes from the B region, formed by the supercage and the narrow neck [Fig. 10(c)]. The α parameters of both single regions increase at low loadings, the increase in α_B being faster [Fig. 10(a)]; the load fraction of region A goes through an increase, followed by a decrease [Fig. 10(b)], which affects the trend of the region A contribution to the overall α_{AB} [Fig. 10(c)].

The trends of the single region α parameters [Fig. 10(a)] can be understood looking at the methane PDF inside the LC and how this evolves with loading. In Fig. 11 we can see the CH_4 isoprobability surfaces (dark areas denote higher probability, i.e., the sorption sites), with increasing loading going from top to bottom, projected on the xy plane (left) and on the xz plane (right). In particular, we can observe how the PDF becomes more homogeneous, over the whole accessible volume, moving from the top couple of plots (a) and (b) to the central couple [plots (c) and (d)]; with enhanced occupancy (in proportion to total load) in the region facing the windows which connect the supercage to the narrow necks. This scenario is responsible for the increase in both the single region α parameters. Moving from the central couple of plots [plots (c) and (d)] to the bottom one [plots (e) and (f)], we see that new sorption sites appear inside the supercage: a site at about half the distance, along the z-direction, between the culs-de-sac and the center of the supercage; and six small sites in the ring facing the MCSs at the center of the supercage. These new sites are responsible for the decrease in the α_B parameter at high loadings. On the other hand, the PDF inside region A becomes more and more homogeneous with loading so that the α_A parameter continues to grow.
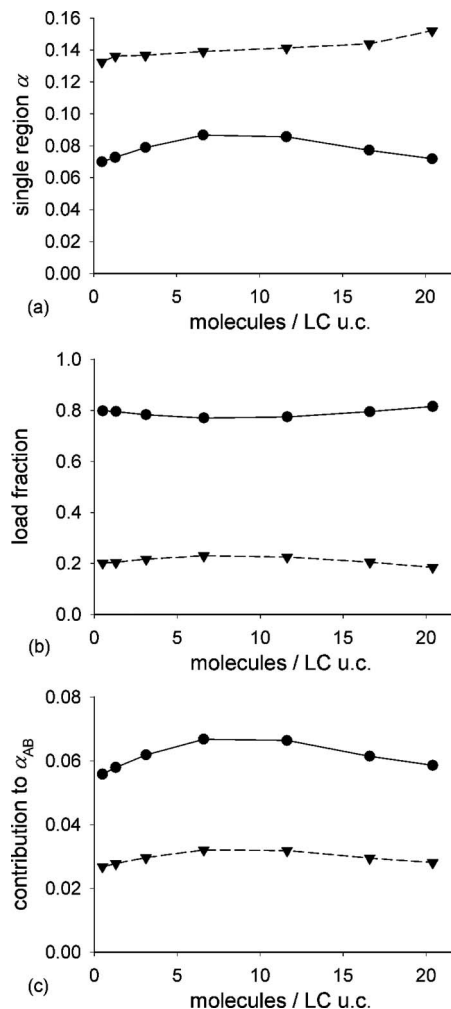

FIG. 10. CH_4 in LC: α parameter (a), load fraction N_A/N_{AB} and N_B/N_{AB} (b), and contribution to α_{AB} (c), from single regions A (triangles) and B (circles) [see Eq. (15)].

For CH_4, the space discretization has been performed surrounding each neck, in the xy plane, with a circle of radius $R_{neck}=0.23$ nm [see Fig. 11(a)]. In these calculations, region A has an extension along the x-direction of $l_A=0.40$ nm, while region B of $l_B=0.83$ nm.

For completeness, we should note that in Eq. (15) each bracket corresponds, respectively, to a portion l_A/l_{AB} and l_B/l_{AB} of α_{AB}; thus we can write $\alpha_A = \alpha_{AB}(l_A/l_{AB}) \times (N_{AB}/N_A)$ and $\alpha_B = \alpha_{AB}(l_B/l_{AB})(N_{AB}/N_B)$, obtaining the following relation:

$$N_A \alpha_A/l_A = N_B \alpha_B/l_B. \quad (16)$$

In systems where the position of the MCS does not change sensibly with loading (constant l_A/l_B), Eq. (16) shows that α_A, α_B, and N_A/N_B (the *load repartition* between the two regions A and B, different from the load redistribution within each single region) are closely bonded together. Coupling together Eqs. (15) and (16), then, we can outline three limit scenarios for an increase in the overall α_{AB} with loading; these are (I) a proportional increase in both α_A and α_B if N_A/N_B is fixed (the new load populates the two regions respecting the previous ratio); (II) a decrease in N_A/N_B (load repartition toward B) with proportional increase in α_A if α_B
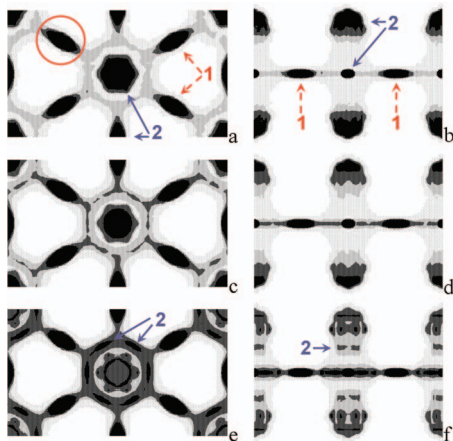
FIG. 11. Isoprobability contours for CH_4 inside the LC pore network (dark areas denote higher probability); xy projection [(a), (c), and (e)] and xz projection [(b), (d), and (f)]. Molecules in LC per unit cell: 0.19 [top: (a) and (b)], 6.6 [center: (c) and (d)], and 20.4 [bottom: (e) and (f)]. The circle enclosing the neck has radius $R_{neck}=0.23$ nm (a). The numbers of the sorption sites denote the two different kinds, distinguished according to the way in which they prevent molecules from reaching the MCSs.

is fixed; and (III) an increase in N_A/N_B (load repartition toward A) with proportional increase in α_B if α_A is fixed. Note that in the limit of infinite concentration we expect N_A/N_B to approach a value close to the ratio between the accessible volumes of the two single regions, V_A/V_B.

3. Carbon dioxide diffusivity

Performing the same analysis for CO_2, we can see (Fig. 12) that the greater contribution to the overall α_{AB} comes again from region B [plot (c)]. The α parameter of region A decrease monotonically, while the one of region B decreases at low loadings and then slightly increases [plot (a)]; at high occupancy there is a small load repartition toward region A [plot (b)], which causes the contribution of region A to the overall α_{AB} to exhibit a decrease at low loadings followed by an increase, in analogy with the profile of the overall contribution coming from region B [plot (c)].

We study the carbon dioxide PDF inside the LC and its evolution with loading. In Fig. 13 we can see the CO_2 isoprobability surfaces; the plots follow the same scheme introduced for CH_4 in Fig. 11. As loading increases, moving from plots (a) and (b) to plots (c) and (d), inside the supercage a new sorption site appears at about half the distance, along the z-direction, between the culs-de-sac and the center of the supercage (as for CH_4). This site is responsible for the initial decrease in the α_B parameter. At the same time, inside the narrow necks, we observe a strengthening of the sorption site (probably due to the sorbate-sorbate interaction), with less molecules crossing the MCS and a consequent decrease of the α_A parameter. At even higher loadings, going from plots (c) and (d) to plots (e) and (f), the sorbate PDF inside the supercage becomes more homogeneous in the region facing the MCS, allowing the slight increase in the α_B parameter. The PDF in the neck, instead, becomes even more structured, with a monotonic decrease of the α_A parameter.

Due to the small size of the necks in the case of the carbon dioxide sorbate, to discretize space we surround each
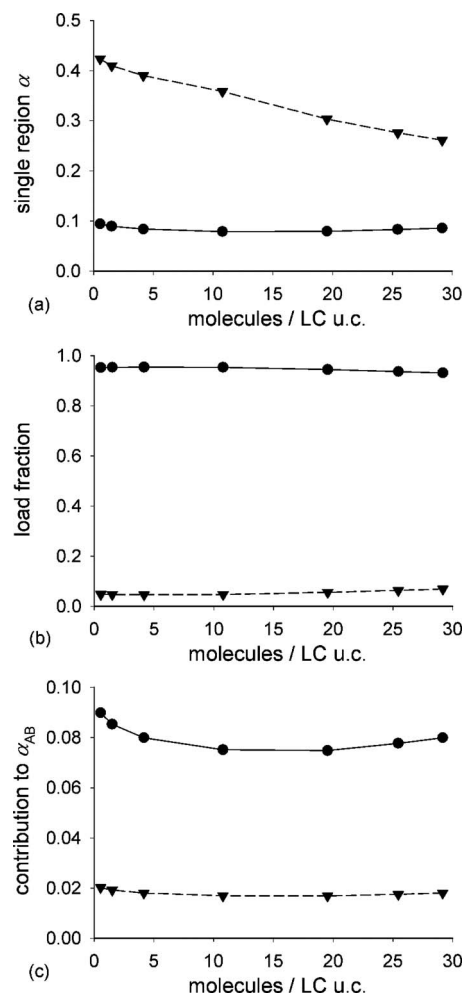

FIG. 12. CO_2 in LC: α parameter (a), load fraction N_A/N_{AB} and N_B/N_{AB} (b), contribution to α_{AB} (c), from single regions A (triangles) and B (circles) [see Eq. (15)].

neck, in the xy plane, with an ellipse having a minor axis of length $R_{neck}=0.13$ nm parallel to the line passing through the centers of the supercages connected by the given neck; the major axis has length $\sqrt{2}R_{neck}$ [see Fig. 13(a)]. Region A has an extent of $l_A=0.225$ nm along the x-direction, while region B has $l_B=1.005$ nm.
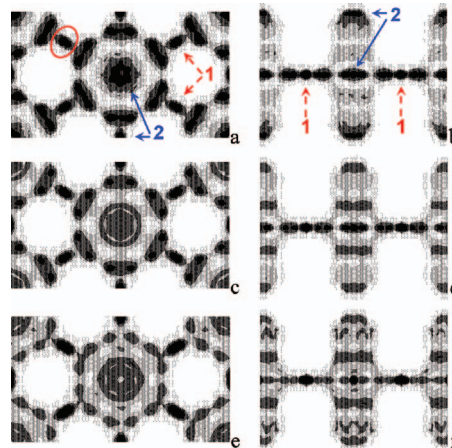

FIG. 13. Same as Fig. 11 for CO_2. Molecules in LC per unit cell: 0.2 [top: (a) and (b)], 10.8 [center: (c) and (d)], and 29.2 [bottom: (e) and (f)]. The necks are bounded using ellipses of minor axis $R_{neck}=0.13$ nm and major axis $\sqrt{2}R_{neck}$ (a).

V. CONCLUSIONS

The DSD method is an extension to periodic media of our previously developed second-order Markov process model. We introduce the concept of MCS to obtain a unique decomposition of the self-diffusion coefficient, along the x-direction, through the α and ζ parameters, according to the relation $D_S = \frac{1}{2}\langle|v_x|\rangle\alpha\zeta$. Here, the α parameter accounts for the efficiency of the thermal speed in bringing about transition across the MCS (fraction of the loading that can see the MCS), while the ζ parameter accounts for the particle-particle collisions and the tortuosity of the system.

Through this DSD method, considerable insight into the physical phenomena governing the dependence of self-diffusivity on loading can be gained. The key point, concerning the diffusivity trend, is the position of the potential wells (sorption sites) with respect to the MCSs, which may enable an increase in the α parameter through the *load redistribution* process. This can potentially lead to a maximum in self-diffusivity, which will manifest itself *if and only if* the growth with loading of the α parameter is faster than the corresponding decrease of the ζ parameter.

Two case studies of systems exhibiting a maximum in the self-diffusivity dependence over loading have been performed. When MCSs are normal to the diffusion coordinate, a maximum can be found (1) in the case of potential wells distributed along the diffusion direction and (2) in the case of potential wells distributed perpendicular to the diffusion direction and located behind uncrossable walls that partly block diffusive progress in the diffusion direction. For completeness, two additional case studies of systems that can by no means present a maximum in the self-diffusivity as a function of loading have been presented.

Subsequently, the DSD method has been applied to a real material, studying the self-diffusivity of CH_4 and CO_2 inside the LC network system of the ITQ-1 zeolite; wherein the first sorbate exhibits a maximum in self-diffusivity as loading increases, while the second does not. In this system the potential wells used in the preceding case studies are replaced by *sorption sites*, which are in most cases of limited spatial extension. The mechanisms creating favorable conditions for a maximum in self-diffusivity, though, remain unchanged. A maximum occurs (1) if the sites *face* the MCSs for the given coordinate direction; and (2) if the sites are screened behind uncrossable walls with respect to the MCSs. The PDFs of the two sorbates in the investigated system are significantly different. For methane, the top and bottom of the supercages constitute sorption sites that are kept away from the main pathways of diffusion [mechanism (2) above]; this results in an increase in the α parameter occurring at low densities, where the ζ parameter exhibits a slow decrease (Henry's regime with few collisions), which allows the appearance of the maximum in the self-diffusivity curve. Carbon dioxide, in contrast, shows a slight increase in the α parameter at higher densities, where ζ drops fast with loading, thus canceling the favorable contribution of the α's growth. These results show to what extent the diffusive behavior of different sorbates varies inside the same sorbent, as a consequence of the location of the sorption sites and their strength with respect to the sorbate-sorbate interactions.

APPENDIX A: DERIVATION OF THE α PARAMETER

Focusing our attention on a single region of extent l in the x-direction, delimited by two consecutive MCSs, i.e., a primitive region, we know that

$$\frac{1}{\tau} = \frac{L}{lN}\frac{2n_{\text{crossings}}}{\Delta t}, \tag{A1}$$

where L is the simulation box length along x and N is the total number of molecules inside the box. The ratio L/l is an integer (by system construction) denoting the number of primitive regions in the simulation box so that lN/L gives the number of molecules within just one of these regions. The number of crossings $n_{\text{crossings}}$ represents the exits from the given region within time Δt through just one MCS; it is multiplied by a factor of 2 since we are interested in the exits per unit time through both boundaries of the given region.

Applying the kinetic theory of gases,[8] at equilibrium we get

$$n_{\text{crossings}} = \Delta t\left(\int_{\text{MCS}} c(x,y,z)dS\right)\left(\int_0^\infty v_x f(v_x)dv_x\right), \tag{A2}$$

where $f(v_x)$ is the velocity probability distribution function along the x-direction, with

$$\langle|v_x|\rangle = 2\int_0^\infty v_x f(v_x)dv_x. \tag{A3}$$

Thus, we can write

$$\frac{1}{\tau} = \frac{L}{lN}\left(\int_{\text{MCS}} c(x,y,z)dS\right)\langle|v_x|\rangle \tag{A4}$$

and remembering that $l/\tau = \langle|v_x|\rangle\alpha$ [Eq. (4)], we obtain $\alpha = (L/N)\int_{\text{MCS}} c(x,y,z)dS$ [Eq. (5)].

APPENDIX B: COMPARISON WITH TST

In this section, we want to outline the similarities and differences between the DSD method and the TST; showing that the theoretical concepts of our method are valid also in the *rare event regime* even though the DSD method cannot be competitive with TST since it needs the computation of the two relevant parameters, α and ζ, in the course of a continuous dynamics simulation (standard time scale limitations associated with MD).
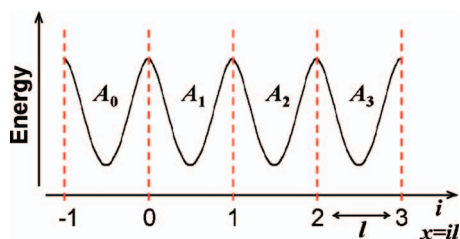
FIG. 14. Energy diagram for a one-dimensional system with identical states A_i and dividing surfaces placed at a distance l from each other along the reaction coordinate x.

We envision a simple one-dimensional periodic system formed by the repetition, along the reaction coordinate x, of identical stable configurations A_i (where the index i enumerates the states), separated by identical energy barriers. The distance between the barriers (dividing surfaces) is l, the barriers being located at $x_i = il$, with $i \in \mathbb{N}$ (see Fig. 14).

We first consider the case where the boundaries of each state are very sharp; thus, we can invoke the TST assumption: every crossing of the dividing surface corresponds to a reactive state change. In this case, TST yields a self-diffusivity

$$D_S = k^{TST} l^2, \tag{B1}$$

where k^{TST} is simply the rate of escape from a given state across only one of its boundary surfaces, e.g., $k^{TST} = k_{A_1 \to A_2}$.[9] In the same conditions, our DSD method gives a diffusivity of

$$D_S = \frac{1}{2} \frac{l}{\tau} \lim_{i \to \infty} \frac{ilP}{1-P},$$

where τ is the mean residence time a particle will spend in a given state before escaping through any of the two boundaries and P is the transmission probability, which depends on the distance il between the two boundaries. When the TST assumption holds, we can remove the limit over states (regions) of bigger extent since the particles will thermalize in their destination state, with minimal correlations between consecutive transmissions. After thermalizing in a given state (loss of memory), the particles will have the same probability to exit from either one of the two boundaries so that $P = 0.5$. The DSD self-diffusivity becomes

$$D_S = l^2/(2\tau), \tag{B2}$$

equivalent to the TST result since, in this formalism, $k^{TST} = 1/(2\tau)$.

Now we relax the TST assumption, allowing, for example, the states to be populated so that some particles may recross a given boundary without thermalizing in the new state; we still assume, however, that there are no correlations between consecutive moves through adjacent states, i.e., no multistate correlated jumps with a particle thermalizing in a state nonadjacent to the one from which it started. In this case the TST theory has been refined introducing a dynamical-correction factor $f_d = 1 - (N_{spur}/N_{tot})$ to remove the spurious recrossing jumps N_{spur} (not contributing to the dif-

fusive process), from the total number of crossings through one dividing surface N_{tot}, thus enabling the computation of an effective rate of crossing $k^{eff} = k^{TST} f_d$. The TST self-diffusivity,[4] in this case, becomes

$$D_S = k^{TST} f_d l^2. \tag{B3}$$

Applying our DSD method in these conditions, we can avoid once again the limit over states of bigger extent and the self-diffusivity is just

$$D_S = \frac{1}{2} \frac{l^2}{\tau} \frac{P}{1-P}.$$

For TST and DSD to give the same results, then it should be $f_d = P/(1-P)$, within the errors inherent in the two methodologies.

If now we raise the temperature of the system, or reduce the height of the energy barriers, a degree of correlation between the successive moves through adjacent states will arise so that a particle may thermalize in a state nonadjacent to the one where it originated. The TST method deals with this problem introducing the concept of a rate constant between two states which are not adjacent in configuration space (multistate system) so that the moves from a given state A_i are decomposed in subgroups according to the various final thermalization states A_j, and a dynamical correction factor is computed independently for each subgroup. This solution extends the range of applicability of TST until a time scale separation exists between the mean time on which the correlated recrossing events occur τ_{corr} (mean time for thermalization), and the mean time for a *reactive crossing* of the dividing surface τ_{rxn} so that $\tau_{corr} \ll \tau_{rxn}$.[9] At high temperatures and/or low energy barriers (e.g., bulk conditions), this time scale separation may disappear and TST becomes inapplicable.

On the other hand, DSD method makes no use of concepts such as time scale separation: the correlations in the consecutive moves are treated coarse-graining together the given space regions (states) to obtain regions of larger extent; e.g., in the system of Fig. 14, the individual regions A_i can be fused together resulting in composite regions $B_i = A_{2i} + A_{2i+1}$. This approach allows the theoretical concepts of our method to hold for all ranges of dynamics, up to the bulk. From this favorable point of view, we note that what appears (and can be conveniently computed) as a recrossing factor in the *infrequent events* time regime, the f_d of TST, is with more generality a value depending on the transmission probability over the whole region or state, the $P/(1-P)$ of DSD; in this broader picture, for example, this value can naturally be bigger than 1. At the same time, we see that the quantity $\zeta = \lim_{i \to \infty}(ilP/(1-P))$ is intensive, which suggests treating it as one single parameter. The term l/τ, then is an intensive quantity as well since its product with ζ equals $2D_S$, and the same is true for $\alpha = (l/\tau)/\langle |v_x| \rangle$.

[1] M. Sant, G. K. Papadopoulos, and D. N. Theodorou, J. Chem. Phys. **128**, 024504 (2008).

[2] M. P. Allen and D. J. Tildesley, *Computer Simulation of Liquids* (Clarendon, Oxford, 1989).

[3] A. Einstein, Ann. Phys. **17**, 549 (1905).

[4] D. Dubbeldam, E. Beerdsen, T. J. H. Vlugt, and B. Smit, J. Chem. Phys. **122**, 224712 (2005).

[5] J. D. Weeks, D. Chandler, and H. C. Andersen, J. Chem. Phys. **54**, 5237 (1971).

[6] M. A. Camblor, A. Corma, M. J. Días-Cabañas, and C. Baerlocher, J. Phys. Chem. B **102**, 44 (1998).

[7] M. Sant, J.-M. Leyssale, G. K. Papadopoulos, and D. N. Theodorou, J. Phys. Chem. B **113**, 13761 (2009).

[8] R. D. Present, *Kinetic Theory of Gases* (McGraw-Hill, New York, 1958).

[9] A. F. Voter and J. D. Doll, J. Chem. Phys. **82**, 80 (1985).